JOURNAL OF THE AMERICAN CHEMICAL SOCIETY

Communication

pubs.acs.org/JACS

Photoinduced Conversion of Methane into Benzene over GaN Nanowires

Lu Li,[†,‡] Shizhao Fan,[‡] Xiaoyue Mu,[†] Zetian Mi,*[,‡] and Chao-Jun Li*[,†]

[†]Department of Chemistry, McGill University, 801 Sherbrooke Street West, Montreal, QC H3A 0B8, Canada

[‡]Department of Electrical and Computer Engineering, McGill University, 3480 University Street, Montreal, QC H3A 0E9, Canada

Supporting Information

ABSTRACT: As a class of key building blocks in the chemical industry, aromatic compounds are mainly derived from the catalytic reforming of petroleum-based long chain hydrocarbons. The dehydroaromatization of methane can also be achieved by using zeolitic catalysts under relatively high temperature. Herein we demonstrate that Si-doped GaN nanowires (NWs) with a 97% rationally constructed *m*-plane can directly convert methane into benzene and molecular hydrogen under ultraviolet (UV) illumination at rt. Mechanistic studies suggest that the exposed *m*-plane of GaN exhibited particularly high activity toward methane C−H bond activation and the quantum efficiency increased linearly as a function of light intensity. The incorporation of a Si-donor or Mg-acceptor dopants into GaN also has a large influence on the photocatalytic performance.

The recent discovery of an enormous amount of shale gas is projected to change the landscape of the chemical industry,[1] since through suitable conversions shale gas may replace the dwindling petroleum resources as a carbon-based feedstock.[2−7] Unfortunately, due to the inert C−H bonds in methane, there has been no easy way of turning shale gas into synthetically useful compounds such as olefins and aromatics,[8] being especially hard for the latter.[9] This caused a major concern of a great shortage of aromatic compounds for shale-gas-based future chemical industry. So far, many efforts have been devoted to the formation of aromatics directly from methane and several efficient heterogeneous catalysts have been developed and well investigated, such as Mo,[10] Zn,[11] and Re[12] supported on ZSM-5 zeolites. However, an elevated temperature (>500 °C), owing to the large positive Gibbs free energy [eq 1], is required to promote the equilibrium conversions of methane.

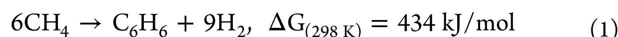

$$6CH_4 \rightarrow C_6H_6 + 9H_2,\ \ \Delta G_{(298\ K)} = 434\ kJ/mol \quad (1)$$

Besides a thermal strategy, another promising approach is to use photoenergy to drive the conversion of methane.[13] Recently, Yoshida et al.[14,15] and Chen et al.[16,17] developed several photocatalysts for methane conversion, respectively, such as SiO_2−Al_2O_3 oxides with highly dispersed Ti, Ga_2O_3, and Zn^+-ZSM-5 zeolite for the methane coupling reaction. However, none of these powdered photocatalysts previously reported can produce aromatic compounds and the methane conversion rate is still low. It is noted that most of these photocatalysts are insulator-supported (SiO_2 or zeolites) materials which have a large band gap and low optical absorption. Nevertheless, the widely used metal oxide semiconductors (such as TiO_2, ZnO, and Cu_2O) are not suitable supports for the methane conversion reaction, simply because they are not stable and the lattice oxygen can be abstracted by the produced hydrogen in the harsh gas−solid environment.[13,17]

GaN, a well-known group III nitride semiconductor, has a direct energy band gap of ∼3.4 eV at rt, which can be further tuned across the entire solar spectrum by incorporating other elements.[18] Compared with metal oxide semiconductors, the controlled n- and p-type doping and the inherent chemical stability, due to the strongly ionic character of the atomic bonds, make GaN a suitable electronically active support for the photocatalytic reaction under harsh conditions.[19] Furthermore, compared with conventional powdered photocatalysts, nanowires (NWs) are highly desirable due to their large surface-to-volume ratios, well-defined surface structures, and superior photoelectrical properties.[20] Consequently, we synthesized nondoped GaN NWs with lengths of 800 nm grown on silicon (111) substrate by plasma-assisted molecular beam epitaxy (MBE) under nitrogen-rich conditions.[21] Scanning electron microscopy (SEM, Figure 1a) and transmission electron microscopy (TEM, Figure 1b and 1c) images of the as-synthesized GaN NWs revealed that the NWs possess hexagonal cross sections and are vertically aligned to the substrate, with the morphology slightly tapered from top to bottom. The electron diffraction pattern (inset of Figure 1c) indicates that the wires are of single crystal wurtzite structure with the growth direction along the *c*-axis, with the top facet of the *c*-plane and lateral facet of *m*-plane. The diameter distribution of the top facets derived from SEM measurements fits well in a logarithmic normal distribution with a mean diameter of $d_{NWs} = 100 \pm 5$ nm (Figure 1d). Figure 1e shows the rt photoluminescence (PL) spectrum of GaN NWs with an intensive peak around 365 nm, corresponding to the band gap of 3.4 eV. To evaluate the photocatalytic performance of the GaN semiconductor comprehensively, we have also prepared GaN thin films (Supporting Information (SI) Figure S1) with a thickness of 650 nm grown on sapphire using AlN as the buffer layer and commercial powdered samples (Figure S2). As shown in Figure 1f, due to the orientated growth on the substrates, the only reflections of GaN NWs and thin films obtained from X-ray diffraction (XRD) measurements are 002 and 004,[22] which further confirms that the top facet of GaN NWs

Received: January 14, 2014
Published: May 14, 2014

ACS Publications © 2014 American Chemical Society

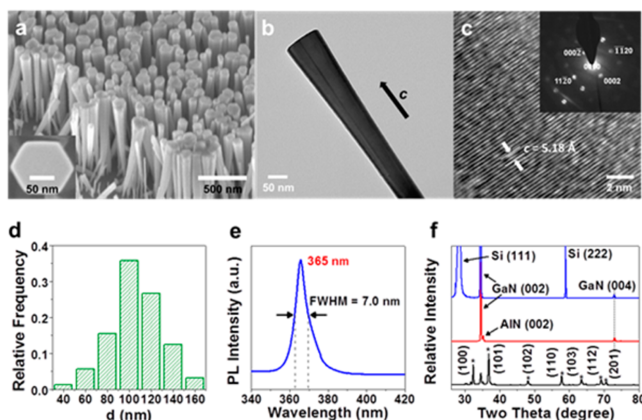

Figure 1. (a) SEM, (b) low- and (c) high-resolution TEM images, (d) diameter distribution, and (e) room temperature PL spectrum of the as-synthesized GaN NWs. The inset of (a) shows the top view of one nanowire. The inset of (c) is the selected area electron diffraction pattern of the lateral facet of one nanowire. The relatively narrow full-width-at-half-maximum (fwhm) of the PL peak suggests that the NWs are strain-free. (f) Powder X-ray diffraction patterns of wurtzite GaN samples in the forms of nanowire, thin film, and powder (from top to bottom).

and thin films is the *c*-plane. The area densities of the NWs and thin films are measured to be 0.1 and 0.4 mg·cm^{-2}, respectively.

The performances of the nondoped GaN materials in different forms for the photocatalytic methane conversion reaction were tested at 5 °C under UV irradiation from a 300-W xenon lamp. To quantitatively evaluate the photocatalytic activities upon irradiation at a longer UV wavelength (UVA and UVB components of sunlight), a set of UV filters (Figure S3) was carefully mounted in the system to completely block wavelengths shorter than 290 nm and longer than 380 nm from the xenon lamp. After the reactions, the GaN NWs were found to show the highest photocatalytic activity for the methane dehydroaromatization reactions among all the GaN samples tested. The catalytic reaction led to the formation of benzene and H_2 with nearly 1:9 stoichiometry, as confirmed by using gas chromatography (GC) and gas chromatography−mass spectrometry (GC-MS) (Figure S4 and Table S1, entry 1). The selectivity for benzene over alternative hydrocarbon products (toluene, ethane, and ethylene) was measured to be 96.5%. Using a series of UV-cut-out filters (Supporting Figure S5), we determined that the minimum photon energy required to drive this reaction over GaN samples corresponds to a wavelength of 360 nm. No conversion was detected under darkness due to the thermodynamic limitation of this reaction (the benzene yield can be estimated to be ca. 0.000007% in the equilibrium at 298 K in our case). Besides GaN NWs, GaN powders (Table S1, entry 2) also showed substantial activity but GaN thin films (Table S1, entry 3) showed negligible photocatalytic activity for methane conversion. This result is interesting since the strong piezoelectric field in GaN thin films can induce effective photoexcited carrier separation, which, together with its single crystallinity, led to enhanced photocatalytic performance for water splitting compared to the powdered sample in our previous work.[23] It implies that the photodriven methane dehydrogenation reaction is governed by not only the photogenerated carriers but also a surface-assisted process.[24]

In this regard, we have comprehensively investigated the structural effect of GaN materials on the photocatalytic performances. The specific surface area of GaN NWs can be calculated to be 5.7 m^2/g by measuring their densities, diameters and lengths. The proportions of the top *c*-plane and lateral *m*-plane are 3% and 97%, respectively. The Brunauer−Emmett−Teller (BET) specific surface area of GaN powders is 3.2 m^2/g, and the TEM image (Figure S6) reveals that the amount of exposed *c*-planes is at the same level as that of exposed *m*-planes on the surface of powdered samples. In the case of GaN thin films, the exposed surface is entirely *c*-plane as confirmed by XRD. Obviously, the surface area of the planar samples is independent of its thickness and mass, but only depends on the dimension of the slice used (10.0 cm^2 in our test). For further comparison, a slice of a short GaN NW sample with a length of 400 nm and an average diameter of 80 nm was prepared (designated as GaN NWs-400) by simply reducing the growth times (Figure S7 and Table S1, entry 4). Figure 2a presents the total surface area of each catalyst used in our test and their corresponding photocatalytic activities for the methane conversion reaction. We can find that the performance of GaN materials depends strongly on their exposed *m*-plane but is not correlated with the *c*-plane. GaN thin films have negligible *m*-plane exposed and hence are unable to convert methane. For comparison, if we performed similar experiments with pure ethylene on the surface of GaN, both the *c*-plane and *m*-plane showed remarkable activities toward the ethylene dehydrogenation reaction (Figure 2b and Table S2). These observations clearly demonstrate that the photodriven methane C−H activation is surface sensitive. In addition, due to the closely spaced nanostructure and large surface area, the equilibrium of CH_4 adsorption on the lateral facets of GaN NWs is not very fast. Thus, an induction period was observed when the UV illumination started immediately upon the exposure of GaN NWs to methane (Figure 3a). For comparison, if GaN NWs were exposed to pure methane in darkness for 1 day prior to the UV illumination, the GaN NWs would show a constant conversion rate during the UV irradiation, and no induction period was observed.

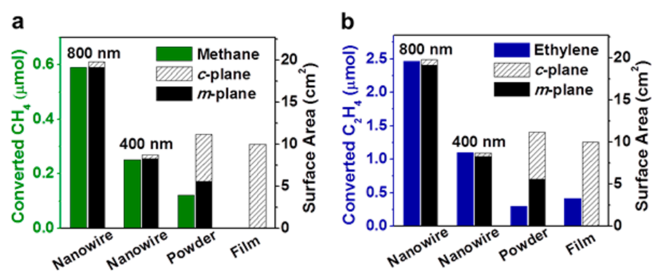

Figure 2. Amount of converted (a) methane and (b) ethylene over various GaN catalysts in different forms and the total surface area of each catalyst used in the test. Reaction conditions were as follows: 0.35 mg of GaN NWs, 0.17 mg of GaN NWs-400, 0.35 mg of GaN powders, and 4.0 mg of GaN thin-films upon 290−380 nm UV irradiation at an intensity of 7.5 mW cm^{-2} for 12 h, respectively.

As shown in Figure 3b, the *m*-plane of ideal wurtzite GaN is composed of binary Ga and N atoms tetrahedrally coordinated with each other, whereas the *c*-plane contains only one type of atom (Ga or N). Previously, the polarization of alkane C−H bonds by Ga^{3+} and adjacent O^{2-} in Ga_2O_3[25] and Ga-ETS-10[17] materials has been proven to be very strong even at rt. Similarly, in the exposed GaN *m*-plane, Ga^{3+} and N^{3-} can interact with the methyl group and H atom of the adsorbed methane molecule, respectively. The GaN lattice consisted of alternating positive-charged Ga and negative-charged N atomic planes, which can

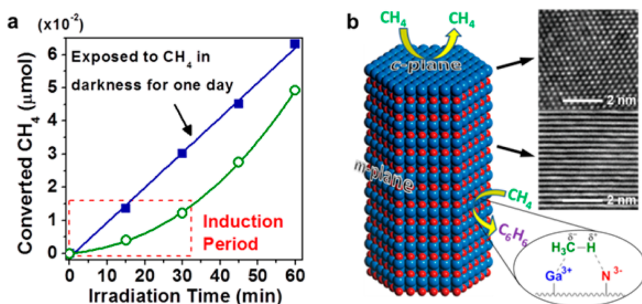

Figure 3. (a) Methane consumption curve upon the initial irradiation time. (b) Schematic diagram for methane C−H bond polarization on the surface of GaN *m*-plane. The insets are high-resolution TEM images of the top *c*-plane and lateral *m*-plane of GaN.

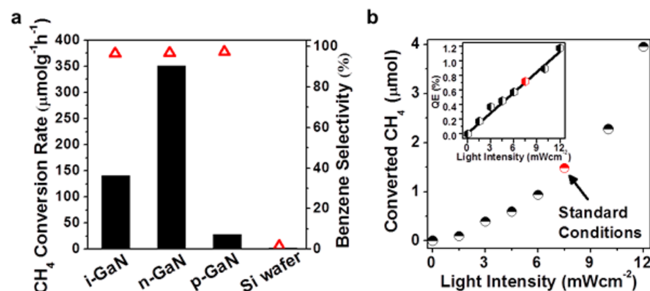

Figure 4. (a) Methane conversion rate and benzene selectivity over a slice of intrinsic GaN NWs, n-type GaN NWs, p-type GaN NWs, and pure Si substrate under UV irradiation (290−380 nm) for 12 h. The area of each slice is 3.5 cm^2. (b) Plot of the methane consumption and quantum efficiency (inset) over n-type GaN NWs in 12 h as a function of the light intensity.

produce strong electrostatic polarization along the *c*-direction and, thus, stretch the methane molecules absorbed on the *m*-plane. Note that the length of the Ga−N bond in the *m*-plane is 1.95 Å, which is significantly longer than the methane C−H bond (1.09 Å) and, hence, highly beneficial to stretching the C−H bond. The polarized methane C−H bond is significantly weakened, promoting its cleavage under UV irradiation. However, on the other hand, the *c*-plane is made up of only Ga (or N) atoms. Owing to the high bond energy of 8.92 eV/atom, the Ga−N bond is extremely hard to break by photons with an energyof <4.3 eV (290 nm) with insertion of its Ga (or N) atom into the methane C−H bond through a classical C−H bond activation mechanism.[8] Consequently, the absence of dipoles in the exposed *c*-plane leaves the C−H bond of the methane molecule intact, which cannot be broken directly by photons.

The incorporation of a trace amount of silicon or magnesium dopants into GaN NWs can significantly alter the Fermi level position and carrier transport properties.[26] To evaluate the effect of doping on the activity of GaN NWs, we have synthesized Si-doped n-type and Mg-doped p-type GaN NWs (Figure S8). The doping density is controlled by tuning the effusion cell temperatures of Si (1350 °C) and Mg (265 °C). The electron and hole concentrations for the Si-doped n-type and Mg-doped p-type GaN NWs were estimated to be on the order of $n = 5 \times 10^{18}$ cm^{-3} and $p = 1 \times 10^{18}$ cm^{-3}, respectively. Figure S9 shows rt PL spectra of the as-synthesized nondoped, Si-doped, and Mg-doped GaN NWs. The PL peak position near ∼365 nm for all three samples is revealed, indicating the band gap of GaN is unchanged after doping. As shown in Figure 4a, the n-type GaN NWs (Table S1, entry 5) exhibited significantly enhanced photocatalytic activity for methane dehydroaromatization compared with the nondoped ones. On the other hand, the activity of p-type GaN NWs (Table S1, entry 6) was severely reduced.

An average methane conversion rate of 325 μmol h^{-1} g^{-1} was achieved after 36-h UV irradiation by using 0.35 mg of n-type GaN NWs (Table S1, entry 7). During the reactions, acetylene was not detected, whereas only small amounts of ethane and ethylene were observed. Thus, a plausible mechanism was proposed (Figure S10). The dehydroaromatization reaction starts with the polarization of methane on the exposed *m*-plane. The initial interaction between adsorbed methane and GaN results in $H^{\delta+}$−$CH_3^{\delta-}$ polarization. Upon UV irradiation, the polarized methane was first heterolytically split into CH_3^- and H^+ on the catalyst surface. A similar heterolytic dissociation of alkane C−H bonds is also evidenced on the surface of gallium oxide[25] or Ga modified zeolites.[27] The photogenerated electron from the GaN semiconductor will migrate to the surface and reduce the proton into a H atom, which then combines to release as H_2 gas. Meanwhile, the methyl group will be oxidized by the photogenerated hole to form a methyl radical, followed by the C−C coupling reaction, forming ethane. The ethylene produced from the ethane dehydrogenation reaction can further go through the cyclization and dehydrogenation process to form benzene. Under the standard conditions described in Table S1, the overall quantum efficiency (benzene molecules produced per photon consumed) between 290 and 380 nm over n-type GaN NWs was calculated to be ca. 0.72%, which is remarkable for a static gas−solid system with poor diffusion. To pinpoint the detailed mechanism, we have tested the catalytic performances of n-type GaN NWs under varying light intensity (Figure 4b). To eliminate the photothermal effect, all the reactions were kept at 5 °C by using a powerful cooling system. The experimental results revealed that the methane conversion rate is proportional to the square of light intensity and the quantum efficiency increases linearly as a function of light intensity. This observation indicates that the process of methane coupling, which is the rate-determining step, requires two photogenerated holes to produce two independent methyl radicals simultaneously, which then couple with each other to form an ethane molecule (a detailed explanation can be found in the SI).[28]

To assess the performance of GaN under the UV light without any filters, Ga_2O_3, an effective photocatalyst reported previously for the methane coupling reaction was prepared and tested for comparison.[15] Using 0.35 mg of the catalysts and 150 μmol of methane, we obtained conversion rates for methane of 148 μmol h^{-1} g^{-1} over Ga_2O_3 powders (Table S1, entry 9) and 63 μmol h^{-1} g^{-1} over GaN powders (Table S1, entry 10) upon UV irradiation without any filters, respectively. In contrast, a conversion rate of methane of 725 μmol h^{-1} g^{-1} was achieved using n-type GaN NWs under identical conditions (Table S1, entry 11).

The performance of GaN NWs can be used repeatedly without noticeable deactivation after several cycles (Figure S11) whereas the crystal structure remained intact (Figure S12). After a long reaction time, a small amount of carbon deposits (polyaromatic and graphitic species) was formed on the surface of GaN NWs which can be completely stripped by the oxygen plasma treatment, as judged by Raman spectroscopy (Figures S13 and S14). More importantly, the lattice Ga^{3+} remained unchanged during the methane conversion reaction. As shown by X-ray photoelectron spectroscopy (Figure S15), neither of the binding energy peaks with maxima at 19.1 (typical for Ga^+) and 17.7 eV

dx.doi.org/10.1021/ja5004119 | J. Am. Chem. Soc. 2014, 136, 7793−7796

(typical for Ga^0) was detected after a long reaction time.[29] Therefore, GaN materials are proven to be highly stable for the methane conversion reaction.

In summary, we have discovered a promising approach to turn shale gas into aromatic compounds powered by photoenergy for the first time. The GaN semiconductor exhibits superior chemical stability and photocatalytic activity for C−H activation of methane at rt.

■ ASSOCIATED CONTENT

Supporting Information

Experimental procedures and analytical data. This material is available free of charge via the Internet at http://pubs.acs.org.

■ AUTHOR INFORMATION

Corresponding Authors

zetian.mi@mcgill.ca

cj.li@mcgill.ca

Notes

The authors declare no competing financial interest.

■ ACKNOWLEDGMENTS

This work was financially supported by the Canada Research Chair (Tier 1) foundation, NSERC, FQRNT, Canada Foundation for Innovation (CFI), and McGill University.

■ REFERENCES

(1) Richard, A. K. *Science* **2010**, *328*, 1624.
(2) Choudhary, V. R.; Kinage, A. K.; Choudhary, T. V. *Science* **1997**, *275*, 1286.
(3) Lunsford, J. H. *Catal. Today* **2000**, *63*, 165.
(4) Periana, R. A.; Mironov, O.; Taube, D.; Bhalla, G.; Jones, C. J. *Science* **2003**, *301*, 814.
(5) Holmen, A. *Catal. Today* **2009**, *142*, 2.
(6) Balasubramanian, R.; Smith, S. M.; Rawat, S.; Yatsunyk, L. A.; Stemmler, T. L.; Rosenzweig, A. C. *Nature* **2010**, *465*, 115.
(7) Schwarz, H. *Angew. Chem., Int. Ed.* **2011**, *50*, 10115.
(8) (a) Bergman, R. G. *Nature* **2007**, *446*, 391. (b) Sun, C.-L.; Li, B.-J.; Shi, Z.-J. *Chem. Rev.* **2011**, *111*, 1293. (c) Yeung, C. S.; Dong, V. M. *Chem. Rev.* **2011**, *111*, 1215. (d) Liu, C.; Zhang, H.; Shi, W.; Lei, A. *Chem. Rev.* **2011**, *111*, 1780. (e) Mkhalid, I. A.; Barnard, J. H.; Marder, T. B.; Murphy, J. M.; Hartwig, J. F. *Chem. Rev.* **2010**, *110*, 890. (f) Lyons, T. W.; Sanford, M. S. *Chem. Rev.* **2010**, *110*, 1147. (g) Young, A. J.; White, M. C. *J. Am. Chem. Soc.* **2008**, *130*, 14090. (h) Wang, D.-H.; Engle, K.-M.; Shi, B.-F.; Yu, J.-Q. *Science* **2010**, *327*, 315. (i) Labinger, J. A.; Bercaw, J. E. *Nature* **2002**, *417*, 507. (j) Crabtree, R. H. *J. Chem. Soc., Dalton Trans.* **2001**, *17*, 2437. (k) Wencel-Delord, J.; Glorius, F. *Nat. Chem.* **2013**, *5*, 369. (l) Jones, W. D. *Top. Organomet. Chem.* **1999**, *3*, 9.
(9) Ahuja, R.; Punji, B.; Findlater, M.; Supplee, C.; Schinski, W.; Brookhart, M.; Goldman, A. S. *Nat. Chem.* **2010**, *3*, 167.
(10) (a) Wang, L.; Tao, L.; Xie, M.; Xu, G. *Catal. Lett.* **1993**, *21*, 35. (b) Wang, D. J.; Lunsford, J. H.; Rosynek, M. P. *J. Catal.* **1997**, *169*, 347. (c) Borry, R. W., III; Kim, Y. H.; Huffsmith, A.; Reimer, J. A.; Iglesia, E. *J. Phys. Chem. B* **1999**, *103*, 5787. (d) Ma, D.; Shu, Y. Y.; Cheng, M. J.; Xu, Y. D.; Bao, X. H. *J. Catal.* **2000**, *194*, 105. (e) Zheng, H.; Ma, D.; Bao, X. H.; Hu, J. Z.; Kwak, J. H.; Wang, Y.; Peden, C. H. F. *J. Am. Chem. Soc.* **2008**, *130*, 3722.
(11) Luzgin, M. V.; Rogov, V. A.; Arzumanov, S. S.; Toktarev, A. V.; Stepanov, A. G.; Parmon, V. N. *Angew. Chem., Int. Ed.* **2008**, *47*, 4559.
(12) Wang, L.; Ohnishi, R.; Ichikawa, M. *J. Catal.* **2000**, *190*, 276.
(13) Yuliati, L.; Yoshida, H. *Chem. Soc. Rev.* **2008**, *37*, 1592.
(14) Yoshida, H.; Matsushita, N.; Kato, Y.; Hattori, T. *J. Phys. Chem. B* **2003**, *107*, 8355.
(15) Yuliati, L.; Hattori, T.; Itoh, H.; Yoshida, H. *J. Catal.* **2008**, *257*, 396.
(16) Li, L.; Li, G. D.; Yan, C.; Mu, X. Y.; Pan, X. L.; Zou, X. X.; Wang, K. X.; Chen, J. S. *Angew. Chem., Int. Ed.* **2011**, *50*, 8299.
(17) Li, L.; Cai, Y. Y.; Li, G. D.; Mu, X. Y.; Wang, K. X.; Chen, J. S. *Angew. Chem., Int. Ed.* **2012**, *51*, 4702.
(18) Han, W. Q.; Fan, S. S.; Li, Q. Q.; Hu, Y. D. *Science* **1997**, *277*, 1287.
(19) Schäfer, S.; Wyrzgol, S. A.; Caterino, R.; Jentys, A.; Schoell, J. S.; Hävecker, M.; Gericke, A. K.; Lercher, J. A.; Sharp, I. D.; Stutzmann, M. *J. Am. Chem. Soc.* **2012**, *134*, 12528.
(20) Garnett, E.; Yang, P. D. *Nano Lett.* **2010**, *10*, 1082.
(21) Nguyen, H. P. T.; Zhang, S.; Cui, K.; Han, X.; Fathololoumi, S.; Couillard, M.; Botton, G. A.; Mi, Z. *Nano Lett.* **2011**, *11*, 1919.
(22) Chuaha, L. S.; Hassana, Z.; Hassana, H. A.; Ahmedb, N. M. *J. Alloys Compd.* **2009**, *481*, 15.
(23) Wang, D.; Pierre, A.; Kibria, M. G.; Cui, K.; Han, X.; Bevan, K. H.; Guo, H.; Paradis, S.; Hakima, A. R.; Mi, Z. *Nano Lett.* **2011**, *11*, 2353.
(24) Zhong, D.; Franke, J. H.; Podiyanachari, S. K.; Blömker, T.; Zhang, H.; Kehr, G.; Erker, G.; Fuchs, H.; Chi, L. *Science* **2011**, *334*, 213.
(25) Kazansky, V. B.; Subbotina, I. R.; Pronin, A. A.; Schlögl, R.; Jentoft, F. C. *J. Phys. Chem. B* **2006**, *110*, 7975.
(26) Zhang, Z.; Yates, J. T., Jr. *Chem. Rev.* **2012**, *112*, 5520.
(27) Luzgin, M. V.; Gabrienko, A. A.; Rogov, V. A.; Toktarev, A. V.; Parmon, V. N.; Stepanov, A. G. *J. Phys. Chem. C* **2010**, *114*, 21555.
(28) Kim, J. D.; Yee, N.; Nanda, V.; Falkowski, P. G. *Proc. Natl. Acad. Sci. U.S.A.* **2013**, *110*, 10073.
(29) Serykh, A. I.; Amiridis, M. D. *Surf. Sci.* **2009**, *603*, 2037.